Available online at www.sciencedirect.com
ScienceDirect
Materials Research Bulletin 41 (2006) 1845–1853
Materials Research Bulletin
www.elsevier.com/locate/matresbu

Phase formation and microwave dielectric properties of Pb^{2+} and Sr^{2+} doped $La_4Ti_9O_{24}$ ceramics

Yuan-Wen Liu, Pang Lin *

Department of Materials Science and Engineering, National Chiao Tung University, Hsinchu 300, Taiwan

Received 14 November 2005; received in revised form 21 February 2006; accepted 13 March 2006
Available online 4 April 2006

Abstract

Phase formation and microwave dielectric properties of the Pb^{2+} and Sr^{2+} doped $La_4Ti_9O_{24}$ ceramics were investigated. Using electron diffraction and Rietveld analysis of the X-ray powder diffraction patterns, we show that the increase in the concentration of Pb^{2+} and Sr^{2+} doping results in the structural transition from $La_4Ti_9O_{24}$ to a $La_{2/3}TiO_3$-type phase (*Ibmm*, No. 74). A change in the crystalline phase considerably affects the microwave dielectric properties, increasing the ε_r from 37 to 130, reducing $Q \times f$ from 25,000 to 5500, and increasing temperature coefficient of the resonant frequency (TCF) from 15 to 300 ppm/°C.

Keywords: A. Ceramics; B. Chemical synthesis; C. Electron diffraction; D. Dielectric properties

1. Introduction

Morris et al. [1] resolved the crystal structure of $La_4Ti_9O_{24}$ using the orthorhombic space group *Fddd* (No. 70) with the lattice parameters $a = 1.41458(1)$ nm, $b = 3.55267(4)$ nm, and $c = 1.45794(1)$ nm. The $La_4Ti_9O_{24}$ lattice includes a complex network of distorted titanium octahedra, sharing corners and edges with one eight-fold and two crystallographically distinct six-fold lanthanum ions in the structure. In a separate work [2], $La_4Ti_9O_{24}$ has been reported to exhibit good microwave dielectric properties, a relative dielectric constant (ε_r) of ~37, a quality factor (Q) of ~3060 at 8.1 GHz, and a temperature coefficient of the resonant frequency (TCF) of ~15 ppm/°C.

$La_{2/3}TiO_3$-type perovskite has recently attracted considerable interest because it has remarkable optical [3,4], electrical [5–10], and microwave dielectric properties [11–14]. The structure of this A-site deficient phase is unstable, because of the high vacancy concentration. Recently, studies of the coexistence of $La_{2/3}TiO_3$-type phase and ferroelectric perovskites ($MTiO_3$, M = Ba^{2+}, Sr^{2+}, Ca^{2+}, and Pb^{2+}) [12,15–18] and $LaNO_3$ (N = Al^{3+}, Ga^{3+}, and Fe^{3+}) [6,11,13,19–21] have been conducted. Importantly, the crystal structure of the $La_{2/3}TiO_3$-type phase has been characterized by a long-range cation/vacancy ordering at the perovskite A-site [5,10,20–22].

The authors previously studied [23,24] the effect of Pb^{2+} on $La_4Ti_9O_{24}$ ceramics. When 1 mol of $La_4Ti_9O_{24}$ ceramics reacts with 3 mol of PbO, the 'parent' phase $La_4Ti_9O_{24}$ is transformed to an $La_{2/3}TiO_3$-type structure with an $(La_{0.44}Pb_{0.33})TiO_3$ composition. Further electron diffraction and XRD refinements showed that $(La_{0.44}Pb_{0.33})TiO_3$ crystallizes in the orthorhombic space group *Ibmm* (No. 74) with $a = 0.55371$ nm, $b = 0.55064$ nm, and

* Corresponding author. Tel.: +886 3 5731848; fax: +886 3 5724727.
E-mail address: Panglin@cc.nctu.edu.tw (P. Lin).

0025-5408/$ – see front matter
doi:10.1016/j.materresbull.2006.03.011

c = 0.77825 nm. Microwave dielectric properties of $(La_{0.44}Pb_{0.33})TiO_3$ are $\varepsilon_r \sim 130$, $Q \sim 1700$, and TCF ~ 320 ppm/°C at resonant frequency f_o = 3.128 GHz.

In this work, $La_4Ti_9O_{24}$ ceramics with Sr^{2+} doping are systematically studied and the differences associated with Pb^{2+} doping are discussed.

2. Experiments

$La_4Ti_9O_{24}$ compounds with various degrees of Pb^{2+} and Sr^{2+} doping (Table 1) were prepared by chemical co-precipitation, as shown in Fig. 1. $La(NO_3)_3{\cdot}6H_2O$ (Strem Chemicals, >99.9%), $TiCl_4$ (Merck, >99%), $Pb(NO_3)_2$ (Showa Chemical, 99.5%), $SrCl_2$ (Showa Chemical, 98%), $H_2C_2O_4$ (Showa Chemical, 99%), and NH_4OH (Tedia Company, ACS grade) were used as the starting chemicals. The concentration of the mixture solution was maintained at ~0.1 M for all syntheses that involve D.I. water as a solvent. The co-precipitated powders were then calcined at 900 °C for 1 h in air. The $(La_{0.44}Pb_{0.33})TiO_3$ and $(La_{0.44}Sr_{0.33})TiO_3$ samples were chemically analyzed by induced coupled plasma spectrophotometer (ICP) to check the stoichiometry (Table 2).

The $La_4Ti_9O_{24}$ ceramic bulks with various degrees of Pb^{2+} and Sr^{2+} doping degrees were prepared in a conventional solid-state reaction to measure microwave dielectric properties. After they had been mixed and calcined at 1000 °C for 1 h in air, the powders were ground and sieved. Polyvinyl alcohol (PVA) was used as binder to press the mixed powders into pellets (9 mm in diameter and 7 mm in thickness) for further sintering at 1300–1350 °C for 4 h in air. (The pellets were surrounded by PbO powder and sintered in a covered platinum crucible to prevent PbO volatilization during sintering.) Then, the sintered pellets were polished to a thickness of 5 mm.

The associated phase was characterized by XRD (MACScience M18XHF diffractometer) with Cu $K\alpha_1$ radiation. The transmission electron microscopy (TEM) study was performed on JEOL 2000FX operating at 200 kV. The relative dielectric constant and quality factor were measured on the basis of the cylindrical cavity method (cavity 1005 CIRC and software CAVITY, Damaskos, Inc.) using a HP8722D network analyzer. Detailed measurement procedures have been described elsewhere [25]. The dielectric property was calculated from the frequency of the $TM_{0\,n\,0}$ resonant modes ($n \geqq 1$). The temperature coefficient of the resonant frequency was measured within the range of 25 and 85 °C, and TCF was defined by $(f_{85} - f_{25})/(f_{25} \times 60)$, where f_{85} and f_{25} are the resonant frequencies at 25 and 85 °C, respectively.

3. Results and discussion

3.1. Thermo-chemical analyses

Fig. 2 plots the DSC and TGA curves of the $(La_{0.44}Pb_{0.33})TiO_3$ and $(La_{0.44}Sr_{0.33})TiO_3$ co-precipitation powders (specimen nos. 5-1 and 5-2, see Table 1). Both samples' TGA curves reveal that an important weight loss occurs in three main steps between 25 and 900 °C. The liberation of occluded water is responsible for the initial weight loss in the temperature range from 25 to 250 °C. The second weight loss of the powders between 250 and 400 °C may be

Table 1
The nominal compositions of the co-precipitated powders

Specimen no.	Nominal composition	Composition (mol)			
		La^{3+}	Ti^{4+}	M = Pb^{2+}	M = Sr^{2+}
1-1	$(La_{0.44}M_{0.11})TiO_{3-\delta}$	4.00	9.00	1.00	0
1-2	$(La_{0.44}M_{0.11})TiO_{3-\delta}$	4.00	9.00	0	1.00
2-1	$(La_{0.44}M_{0.17})TiO_{3-\delta}$	4.00	9.00	1.50	0
2-2	$(La_{0.44}M_{0.17})TiO_{3-\delta}$	4.00	9.00	0	1.50
3-1	$(La_{0.44}M_{0.22})TiO_{3-\delta}$	4.00	9.00	2.00	0
3-2	$(La_{0.44}M_{0.22})TiO_{3-\delta}$	4.00	9.00	0	2.00
4-1	$(La_{0.44}M_{0.28})TiO_{3-\delta}$	4.00	9.00	2.50	0
4-2	$(La_{0.44}M_{0.28})TiO_{3-\delta}$	4.00	9.00	0	2.50
5-1	$(La_{0.44}M_{0.33})TiO_3$	4.00	9.00	3.00	0
5-2	$(La_{0.44}M_{0.33})TiO_3$	4.00	9.00	0	3.00

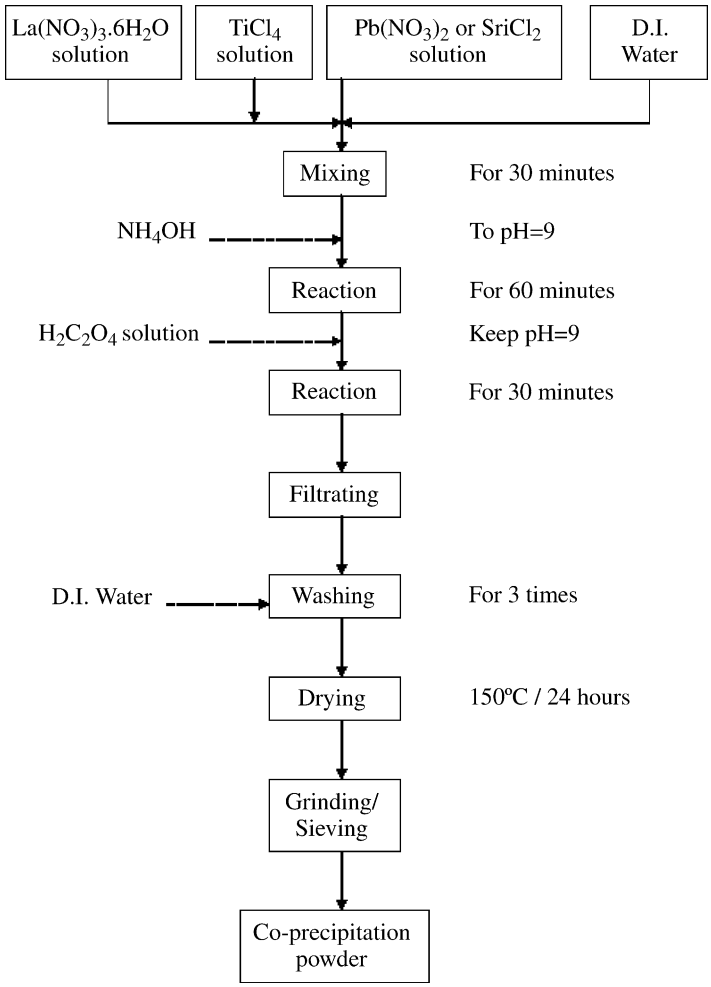

Fig. 1. Schematic co-precipitation preparation of La–Pb–Ti–O and La–Sr–Ti–O powders.

caused by the decomposition of the hydroxyl group and oxalate. The third weight loss in the temperature range 400–800 °C may be caused by the decomposition of the carboxyl group. Complete decomposition occurred at about 900 °C.

Two major differences were observed between the TGA curves of the $(La_{0.44}Pb_{0.33})TiO_3$ and $(La_{0.44}Sr_{0.33})TiO_3$ co-precipitation powders. First, in the temperature range from 25 to 250 °C, $(La_{0.44}Sr_{0.33})TiO_3$ loses more weight (∼15%) than $(La_{0.44}Pb_{0.33})TiO_3$ (∼8%), perhaps because in the formation of $Sr(OH)_2{\cdot}8H_2O$ [26] in the $(La_{0.44}Sr_{0.33})TiO_3$ co-precipitation powder, an increase in the amount of water of crystallization increases the weight lost during this period. The $(La_{0.44}Pb_{0.33})TiO_3$ exhibited another marked weight loss when the temperature was above 1100 °C, but the $(La_{0.44}Sr_{0.33})TiO_3$ sample exhibited no such loss. This phenomenon may be associated with the evaporation of Pb^{2+} due to the fact that the Sr^{2+} is more stable than Pb^{2+} in high temperature.

Table 2
ICP analysis of $La_{0.44}Pb_{0.33}TiO_3$ and $La_{0.44}Sr_{0.33}TiO_3$ on different stages of thermal treatment

Analyzed samples	$La_{0.44}Pb_{0.33}TiO_3$ (molar ratio of La:Pb:Ti)	$La_{0.44}Sr_{0.33}TiO_3$ (molar ratio of La:Sr:Ti)
Initial mixture of aqueous solution	0.439:0.332:1	0.439:0.329:1
Co-precipitated powder	0.439:0.332:1	0.439:0.329:1
Calcined powder at 900 °C/1 h	0.439:0.328:1	0.439:0.329:1

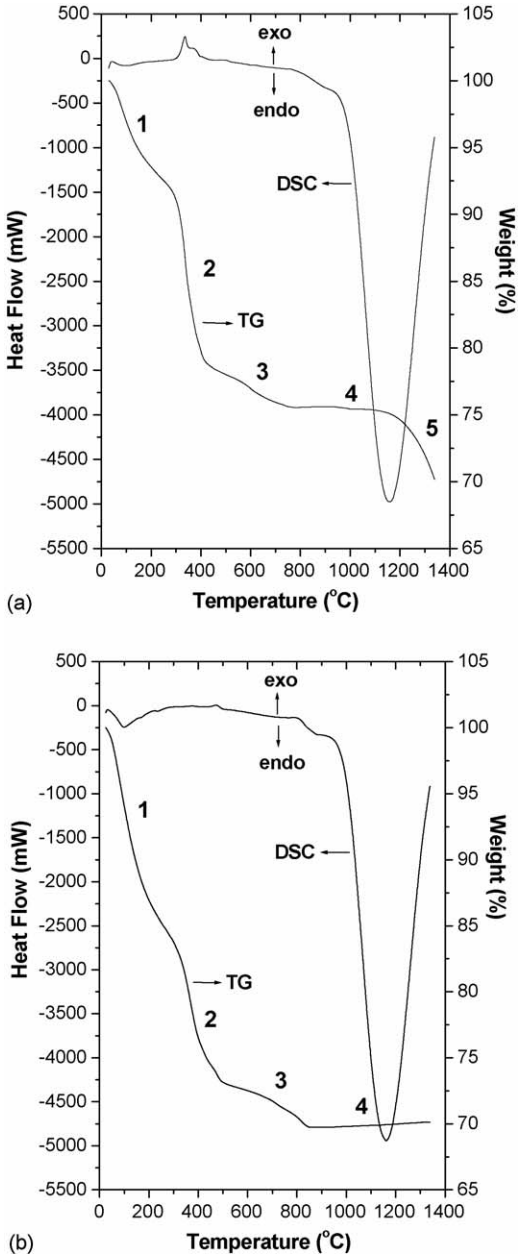

Fig. 2. DSC and TGA curves of: (a) $La_{0.44}Pb_{0.33}TiO_3$ and (b) $La_{0.44}Sr_{0.33}TiO_3$ co-precipitation powders.

The other difference was observed between the DSC curves of the $(La_{0.44}Pb_{0.33})TiO_3$ and $(La_{0.44}Sr_{0.33})TiO_3$ co-precipitation powders in the temperature range from 300 to 400 °C. An obvious exothermic peak was found in the $(La_{0.44}Pb_{0.33})TiO_3$ sample, but not found in the $(La_{0.44}Sr_{0.33})TiO_3$ sample. The exothermic peak may be caused by the decomposition of the PbC_2O_4 [27,28] in the $(La_{0.44}Pb_{0.33})TiO_3$ co-precipitation powder. Both samples' DSC curves included a major endothermic peak observed at around 1150 °C, indicating phase formation during this period.

3.2. Crystalline phase analyses

Fig. 3 presents XRD patterns of the co-precipitation powders calcined at 900 °C, indicating an increase in the proportion of the $La_{2/3}TiO_3$-type phase with the Pb^{2+} and Sr^{2+} doping. Fig. 3a reveals that when the Pb^{2+} doping

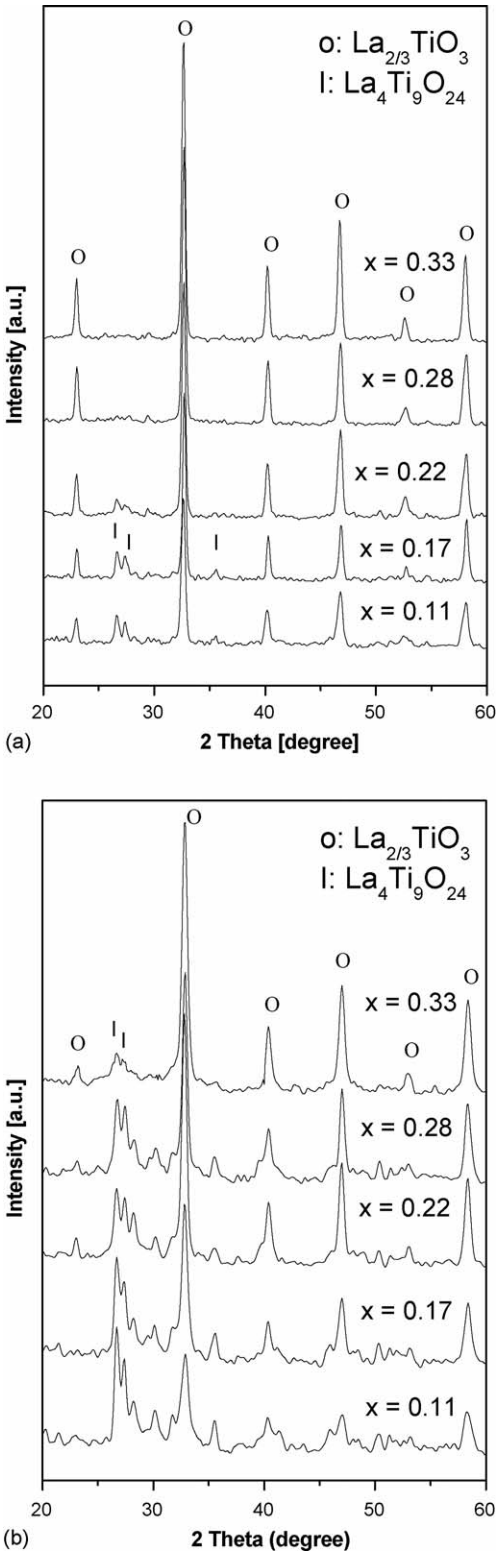

Fig. 3. XRD patterns of co-precipitated powders (a) $(La_{0.44}Pb_x)TiO_3$ and (b) $(La_{0.44}Sr_x)TiO_3$ calcined at 900 °C for 1 h in air with different concentrations.

approaches 3 mol, the $La_{2/3}TiO_3$-type structure becomes the dominant phase. However, in Fig. 3b, the sample doped with 3 mol of Sr^{2+} exhibits some remaining crystalline $La_4Ti_9O_{24}$, which seemed to have a pure $La_{2/3}TiO_3$-type crystalline structure, doping with Sr^{2+} required more energy than doping with Pb^{2+}.

Figs. 4 and 5 present the TEM micrographs and the corresponding selected-area electron diffraction (SAED) patterns of $(La_{0.44}M_{0.33})TiO_3$ (M = Pb, Sr) calcined at 900 °C. The size of the particles of $(La_{0.44}Pb_{0.33})TiO_3$ and $(La_{0.44}Sr_{0.33})TiO_3$ calcined powders is similar (~250 nm; see Figs. 4a and 5a). Figs. 4b and 5b present the $[-1\ 1\ 0]_p$-zone SAED patterns of $(La_{0.44}M_{0.33})TiO_3$ (M = Pb, Sr) (the subscript 'p' denoting cubic perovskites). Both the samples' diffraction patterns include extra weak reflections, indicating an orthorhombic superlattice with $a \sim b \sim 0.55\,\text{nm} \sim \sqrt{2}a_p$ and $c \sim 0.77\,\text{nm} \sim 2a_p$ (a_p, the prototypical lattice parameter of cubic perovskites). Furthermore, the indices of the weak reflections are compatible with the space group *Ibmm* (No. 74).

The Rietveld analysis (Rietica software) [29] is then conducted on the XRD patterns of $(La_{0.44}M_{0.33})TiO_3$ (M = Pb, Sr) using space group *Ibmm* (No. 74). Table 3 shows the refined lattice parameters. It reveals that the crystalline

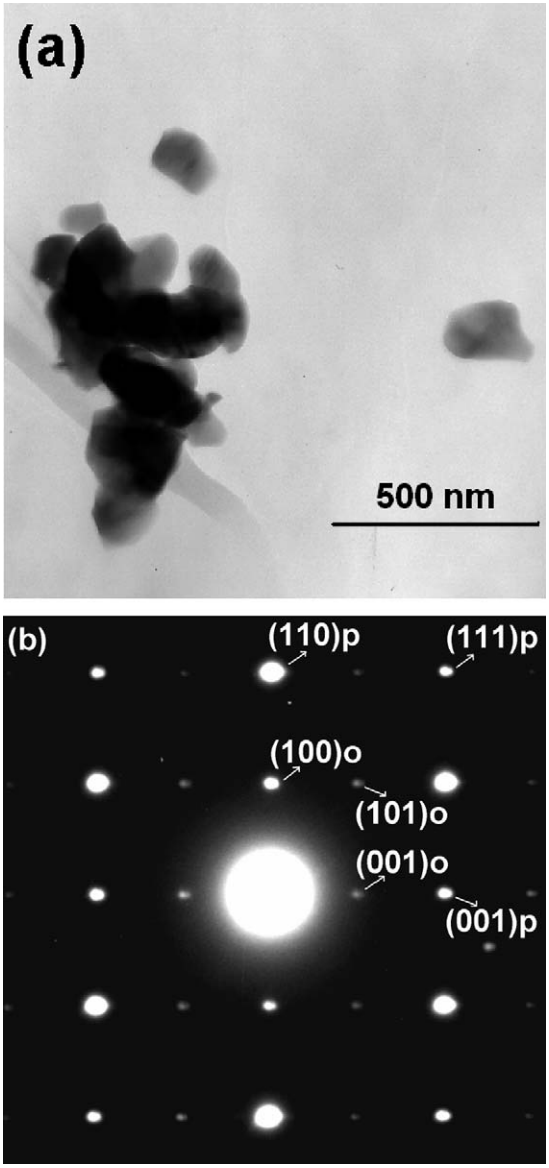

Fig. 4. (a) TEM image of the $(La_{0.44}Pb_{0.33})TiO_3$ powder calcined at 900 °C and (b) the $[-1\ 1\ 0]_p$-zone SAED pattern of $(La_{0.44}Pb_{0.33})TiO_3$. The subscript 'o' represents the orthorhombic superstructure of the corresponding SAED pattern.

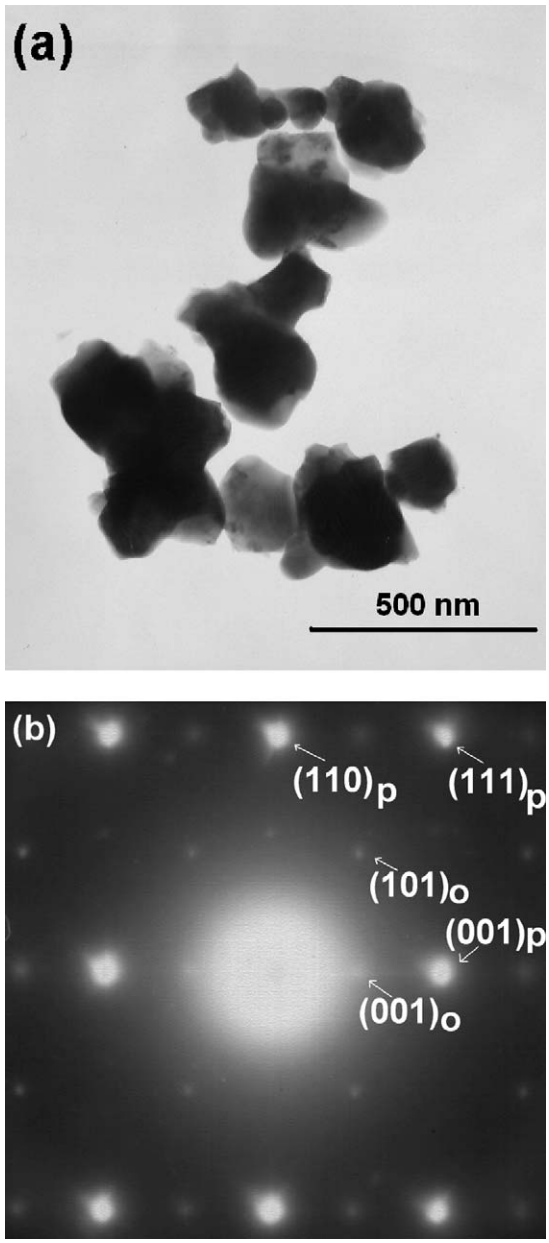

Fig. 5. (a) TEM image of the $(La_{0.44}Sr_{0.33})TiO_3$ powder calcined at 900 °C and (b) the $[-1\ 1\ 0]_p$-zone SAED pattern of $(La_{0.44}Sr_{0.33})TiO_3$. The subscript 'o' represents the orthorhombic superstructure of the corresponding SAED pattern.

$(La_{0.44}Sr_{0.33})TiO_3$ is slightly smaller than $(La_{0.44}Pb_{0.33})TiO_3$, perhaps because of the difference between the sizes of ion Pb^{2+} ($r = 0.118$ nm, CN = 6) and Sr^{2+} ($r = 0.116$ nm, CN = 6).

3.3. Microwave properties analyses

Sintered $La_4Ti_9O_{24}$ bulks (>97% of the theoretical density) with different Pb^{2+} and Sr^{2+} doping degrees were prepared to study the effect of Pb^{2+} and Sr^{2+} doping on the microwave properties of the 'parent' phase $La_4Ti_9O_{24}$. Fig. 6 presents the microwave dielectric properties of the thus-prepared samples at resonant frequency $f_o \sim 3$ GHz. The results reveal a strong relationship between the concentration of dopants (Pb^{2+} and Sr^{2+}) (i.e., the intensity of the $La_{2/3}TiO_3$-type phase) and the properties measured. In Fig. 6a, the ε_r values of the Pb^{2+} and Sr^{2+} doping samples

Table 3
The Rietveld refinement results

	$La_{0.44}Pb_{0.33}TiO_3$	$La_{0.44}Sr_{0.33}TiO_3$
2 theta range (°)	20–80	
Step size (°)	0.02	
Step time (s)	0.5	
Crystal class	Orthorhombic	
Space group	*Ibmm* (No. 74)	
a (nm)	0.55371	0.55185
b (nm)	0.55064	0.54854
c (nm)	0.77825	0.76910
V (nm^3)	0.23728	0.23282
Calculated density (g/cm^3)	6.018	5.059

increase with the concentration of dopants, and the ε_r value of $(La_{0.44}Pb_{0.33})TiO_3$ ($\varepsilon_r \sim 130$) exceeds that of $(La_{0.44}Sr_{0.33})TiO_3$ ($\varepsilon_r \sim 80$). In Fig. 6b, the $Q \times f$ drop as the extent of Pb^{2+} and Sr^{2+} doping increases, and the $Q \times f$ values of the Pb^{2+} doped samples are lower than that of Sr^{2+} doped samples. Fig. 6c presents the TCF property of the sintered bulks, and both Pb^{2+} and Sr^{2+} doping samples have positive TCF values. The effect of Pb^{2+} doping on TCF value is significantly stronger than that of Sr^{2+} doping.

The difference between the microwave dielectric properties of Pb^{2+} and Sr^{2+} doping may be governed by the stereochemical activity [30] of the $6s^2$ lone-pair electrons of Pb^{2+} and the fact that Pb^{2+} is larger than Sr^{2+}, which results in a higher internal stress of Pb^{2+} doped crystalline compared to Sr^{2+} doped crystalline. The higher internal

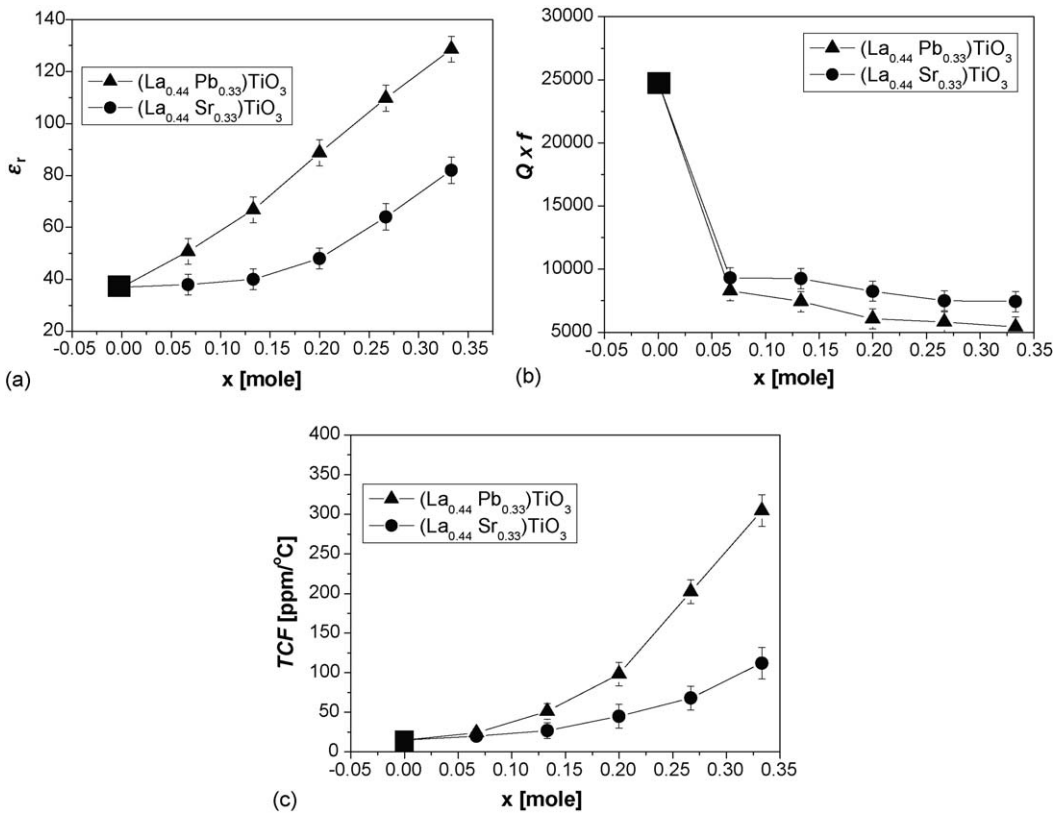

Fig. 6. (a) Relative dielectric constant ε_r, (b) quality factor multiply frequency $Q \times f$, and (c) temperature coefficient of the resonant frequency (TCF) of $La_4Ti_9O_{24}$ ceramics (at $f_o \sim 3$ GHz) with different Pb^{2+} and Sr^{2+} doping sintered at 1300–1350 °C for 4 h. Values for $La_4Ti_9O_{24}$ ceramics marked with the cubic symbol were taken from Ref. [2].

stress may cause the Pb^{2+} doped crystal structure to be more distorted. This phenomenon may have an effect on the difference of microwave dielectric properties between Pb^{2+} and Sr^{2+} doping.

4. Conclusions

The structures of $La_4Ti_9O_{24}$ ceramics with Pb^{2+} and Sr^{2+} dopants were investigated. The crystalline intensity of the $La_{2/3}TiO_3$-type phase increased significantly with the Pb^{2+} and Sr^{2+} doping concentration. Further electron diffraction and XRD refinements indicated that $(La_{0.44}Pb_{0.33})TiO_3$ and $(La_{0.44}Sr_{0.33})TiO_3$ crystallize with the orthorhombic space group *Ibmm* (No. 74). A change in the crystalline phase markedly affects the microwave dielectric properties, increasing the ε_r from 37 to 130, reducing $Q \times f$ from 25,000 to 5500, and increasing TCF from 15 to 300 ppm/°C.

Acknowledgement

The authors thank Dr. M.-W. Chu of National Taiwan University Center for Condensed Matter Sciences (Taiwan) for helpful discussion.

References

[1] R.E. Morris, J.J. Owen, A.K. Cheetham, J. Phys. Chem. Solids 56 (1995) 1297.
[2] J. Takahashi, K. Kageyama, K. Kodaira, Jpn. J. Appl. Phys. 32 (1993) 4327.
[3] D.A. Crandles, T. Timusk, J.D. Garrett, J.E. Greedan, Phys. Rev. B 49 (1994) 16207.
[4] J.K. Park, C.H. Choi, H.D. Park, S.Y. Choi, J. Mater. Res. 16 (2001) 2568.
[5] M.J. MacEachern, H. Dabkowska, J.D. Garrett, G. Amow, W. Gong, G. Liu, J.E. Greedan, Chem. Mater. 6 (1994) 2092.
[6] H. Yoshioka, S. Kikkawa, J. Mater. Chem. 8 (1998) 1821.
[7] W.H. Jung, J. Mater. Sci. Lett. 18 (1999) 1181.
[8] W.H. Jung, H. Wakai, H. Nakatsugawa, E. Iguchi, J. Appl. Phys. 85 (2000) 2560.
[9] H. Yoshioka, J. Am. Ceram. Soc. 85 (2002) 1339.
[10] A.I. Ruiz, M.L. López, C. Pico, M.L. Veiga, J. Solid State Chem. 163 (2002) 472.
[11] H. Yoshioka, Jpn. J. Appl. Phys. 33 (1994) L945.
[12] I.S. Kim, W.H. Jung, Y. Inaguma, T. Nakamura, M. Itoh, Mater. Res. Bull. 30 (1995) 307.
[13] D. Suvorov, M. Valant, S. Škapin, D. Kolar, J. Mater. Sci. 33 (1998) 85.
[14] A.N. Salak, M.P. Seabre, V.M. Ferreira, J. Eur. Ceram. Soc. 23 (2003) 2409.
[15] H. Sasaki, Y. Matsuo, J. Am. Ceram. Soc. 48 (1965) 434.
[16] H. Sasaki, Y. Matsuo, Ceram. Bull. 51 (1972) 164.
[17] T.Y. Tien, F.A. Hummel, Trans. Br. Ceram. Soc. 66 (1967) 233.
[18] H. Yoshioka, J. Mater. Res. 9 (1994) 2133.
[19] S. Škapin, D. Kolar, D. Suvorov, J. Am. Ceram. Soc. 76 (1993) 2359.
[20] D. Hanžel, D. Hanžel, W. Meisel, V. Kraševec, Hyperfine Interact. 92 (1994) 1019.
[21] H.J. Lee, H.M. Park, Y.K. Cho, J. Am. Ceram. Soc. 86 (2003) 1395.
[22] A.I. Ruiz, M.L. López, M.L. Veiga, C. Pico, J. Solid State Chem. 148 (1999) 329.
[23] Y.W. Liu, P. Lin, Mater. Chem. Phys. 92 (2005) 98.
[24] Y.W. Liu, P. Lin, M.W. Chu, J. Mater. Sci., in press.
[25] N. Damaskos, B.J. Kelsall, Microwave J. 38 (1995) 140.
[26] W.F. Linke, Solubilities of Inorganic and Metal-Organic Compounds, D. van Nostrand Co., New Jersey, 1958.
[27] H.L. Clever, F.J. Johnston, J. Phys. Chem. Ref. Data 9 (1980) 751.
[28] M. Pereira, P.Q. Mantas, J. Eur. Ceram. Soc. 18 (1998) 565.
[29] B. Hunter, LHPM-Rietveld, ANSTO: Australia, 2000.
[30] B. Noheda, D.E. Cox, G. Shirane, J.A. Gonzalo, L.E. Cross, S.-E. Park, Appl. Phys. Lett. 74 (1999) 2059.